Effects of nanoscale thickness and elastic nonlinearity on measured mechanical properties of polymeric films

B. Oommen, K.J. Van Vliet *

Department of Materials Science and Engineering, Massachusetts Institute of Technology, Room 8-237, 77 Massachusetts Avenue, Cambridge, MA 02139, USA

Abstract

Scanning probe microscope-enabled nanoindentation is increasingly reported as a means to assess the mechanical properties of nanoscale, compliant material volumes such as polymeric films and bio-membranes. It has been demonstrated experimentally that the Hertzian contact model developed for linear elastic materials of semi-infinite thickness fails to accurately predict the nominal elastic modulus E for polymeric thin films, consistent with limitations identified for comparably rigid metal and ceramic thin films. Here we employ computational simulations based on experimental parameters for compliant polyelectrolyte films, in order to separate limitations of such analysis due to the finite material thickness from those due to nonlinear constitutive relations approximating polymer deformation. We thus identify the range of strains, strain rates, and material thickness for which a modified Hertzian solution can accurately predict the elastic stiffness of polymeric films of nanoscale (<100 nm) thickness from scanning probe microscope-enabled nanoindentation experiments.
© 2006 Elsevier B.V. All rights reserved.

1. Introduction

Nanoindentation is increasingly utilized to estimate the mechanical properties of polymeric films of nanometer-scale thickness. Applications of such films range from bioengineering via synthetic cell substrata [1,2] to insulating layers in integrated circuits [3]. In the context of biological applications, the mechanical compliance of these nanoscale films affects cell functions ranging from cellular differentiation to cellular proliferation to apoptosis (programmed cell death) [4–7]. As scanning probe microscopes (SPMs) exhibit the load and displacement resolution/maxima to deform compliant materials such as polymeric films, SPM-enabled nanoindentation is increasingly reported as a means to assess the mechanical properties of such nanoscaled materials. Most experimental studies to date have applied the Hertzian elastic contact model developed for extraction [8] of Young's elastic modulus E of linear elastic, semi-infinite materials from the nanoindentation load–depth (P–h) response. However, care must be taken in applying this model to nonlinear elastic materials of finite thickness, such as synthetic polymeric films and biological tissues or cells.

Studies in metallic and ceramic thin films have established that E calculated from the nanoindentation response is very strongly influenced by the thin film thickness and substrate mechanical properties, due chiefly to the transfer of contact-induced stresses to the film/substrate interface and to the substrate itself [3,6]. This influence of the underlying substrate on calculated mechanical properties has been addressed by several investigators, chiefly for sharp, self-similar (e.g., conical) indenter geometries for which contact stresses decay sharply with distance from the indenter [9–12]. To capture only the response of the film, it is common to limit the indentation depth to less than 10% of the film thickness — a purely empirical estimate which varies as a function of elastic and plastic mismatch between the film and substrate [13]. However, as an increasing number of applications require film thickness and/or microstructural inhomogeneities of <100 nm length scales, it is desirable experimentally to relax this constraint and still obtain accurate estimates of polymer mechanical properties.

* Corresponding author.
  E-mail address: krystyn@mit.edu (K.J. Van Vliet).

Due to the inherent geometric nonlinearity of such multiaxial contact, there currently exists no convenient, closed-form solution for the contact of mechanically compliant (and/or nonlinear elastic) samples of finite thickness. Dimitriadis et al. addressed the failure of Hertzian contact mechanics to estimate E from the loading portion of the $P–h$ indentation response for compliant samples of finite thickness, and offered a modified model including a film thickness correction [5]. This model derives the Green's function for a sample of finite thickness bonded to the substrate. The integral equations are satisfied by a computed, effective pressure profile acting on the Hertzian contact area. The model assumes an appropriate range of sample thickness t and indentation depth h for a given spherical indenter probe radius. This is based on the assumption that, for a material to behave as a linear elastic solid, the maximum nominal strains should not exceed 10%, or $h \leq 0.1t$. These models are based on the early work of Chen et al., which primarily addresses the problem of stresses induced in multilayer media that is well-adhered to the substrate [14,15]. Investigations for understanding the effect of finite thickness on estimations of elastic modulus E have shown a different dependency on Poisson's ratio v compared to the models proposed by Dimitriadis et al. [16]. Mahaffy et al. revised this model to include poorly adhered films [26] and more conservative corrections for finite thickness to determine experimentally the complex elastic modulus and v of mammalian cells via SPM-enabled nanoindentation. Although the details of these three models differ, they all address the error in finite thickness in accurate determination of E via contact-based measurements on thin, compliant polymer films.

Engler et al. showed that the experimental $P–h$ responses agree well with the thickness-corrected Hertzian elastic cone model proposed by Dimitriadis et al., for the specific case of polyacrylamide hydrogels of thickness $t = 5\,\mu m$ for a maximum indentation depth of $h = 3\,\mu m$ [7]. In contrast, Ludovic et al. [17] have demonstrated that E for polyelectrolyte multilayers (PEM) of micrometer-scale thickness is a function of t when calculated from SPM-enabled indentation, even when this thickness correction is applied to the linear elastic Hertzian elastic sphere model. Finally, Thompson et al. have shown that E calculated from SPM-enabled spherical nanoindentation of hydrated, nanoscale PEM films ($t < 200\,nm$) agrees well with the elastic moduli calculated from other independent experimental techniques and by other researchers for similar PEMs, even in the absence of a thickness correction to the Hertzian model [4].

These contrasting results in polymer films of different compositions and thicknesses highlight an important question: Is the E of a nanoscale polymer film measured via SPM-enabled indentation an intrinsic mechanical property of the material, or an artifact due to combinations of finite thickness, large applied strains, and the inherent nonlinear elasticity of the polymeric material? This issue becomes critical as polymers of decreasing physical dimensions are synthesized and characterized for mechanics–critical applications ranging from biological substrata to low-dielectric constant insulators in integrated circuits. Computational simulations such as finite element analysis (FEA) can be used to analyze the mechanics of deformation for thin films confined to substrates during nanoindentation. For example, stress evolution beyond the elastic limit has been simulated via FEA for layered metallic (titanium/aluminum) thin films [18]. Here we simulate the spherical nanoindentation of polymeric thin films to analyze the deformation field behavior as a function of stress, film thickness, and material constitutive model. Although FEA simulations are continuum-based and therefore inherently independent of length scale, such a study provides important information about the changes in stress and strain fields, and thus estimated mechanical properties, as measured via nanoindentation when the polymer film thickness is reduced to the nanoscale and/or is idealized as a (non)linear elastic material. In practice, structural length scales ($\geq 10\,nm$) other than polymer film thickness exist, such as block copolymer domain size, crystalline diameter in semicrystalline polymers, second-phase particle size in polymeric nanocomposites, and distance between chemical or physical crosslinks in amorphous or hydrated (bio)polymer networks. Therefore, it is useful to consider the effects of finite thickness and material nonlinearity separately from these structural aspects of polymeric films that will affect the validity of a continuum-based mechanical analysis.

2. Simulation details

Fig. 1 shows the finite element model mesh and boundary conditions for the simulations reported herein. This model included 34,476 nodes and 34,104 four-noded axisymmetric elements, and was analyzed via the general purpose finite element software ABAQUS [19]. Both the material films and the spherical indenter exhibit axial symmetry, and are thus considered in a two-dimensional simulation. The indenter was modeled as an infinitely rigid material of radius $R = 25\,nm$, which is consistent with the nominal apex radius of Si_3N_4 pyramidal cantilevers used in SPM-enabled nanoindentation [4], while the material films are modeled using linear elastic and, separately, hyperelastic constitutive relations for film thicknesses of 50, 175, 300, 600, and 1000 nm. The distal conical portion of the cantilevered indenter is not modeled in these simulations, as the typical maximum indentation depth implemented in related experiments [4] and in these simulations is less than R [4]. The contact between the indenter and the material film is assumed to be frictionless, and the nodes at the film/substrate interfaces are modeled as rigidly fixed, based on the assumption that the polymeric film is rigidly bonded to an infinitely rigid (or comparably so) substrate. A displacement controlled analysis is implemented to simulate the nanoindentation, and the output
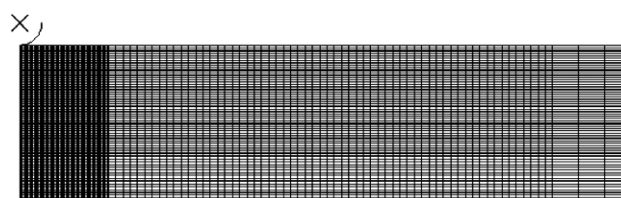

Fig. 1. Finite element model used in simulations of polymer film indentation.
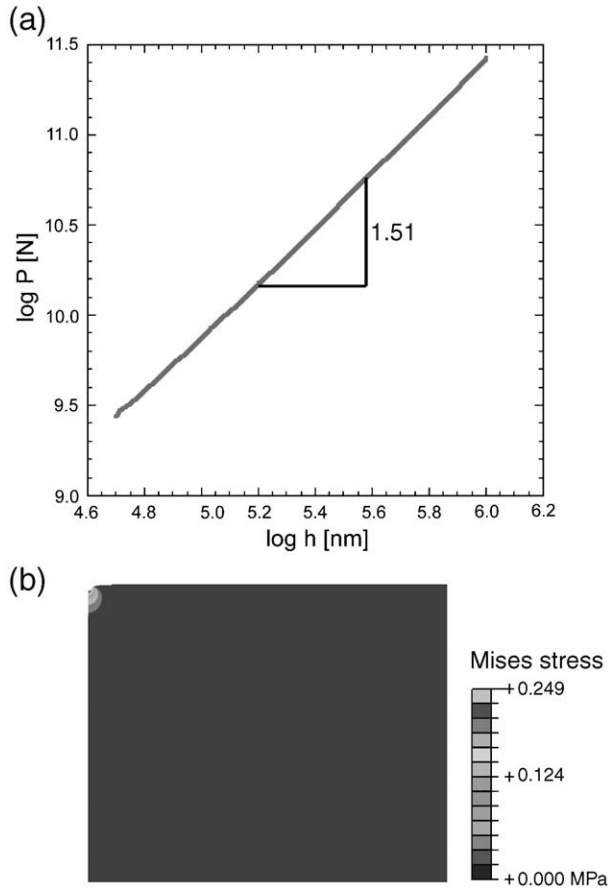
(a)

(b)

Fig. 2. Finite element response of elastic film of thickness $t=1000$ nm and $E=0.5$ MPa: (a) Hertzian prediction of spherical elastic contact given by Eq. (1) is obeyed. (b) Von Mises stress distribution at maximum depth $h=20$ nm.

extracted from the simulations is that of the loading force P corresponding to the indentation depth h at each timepoint; quasistatic loading is thus assumed. The maximum indentation depth h_{max} for all simulations is 20 nm, except for the model for $t=50$ nm where $h_{max}=17.5$ nm was the maximum depth at which the FEA stiffness matrix converged for the given mesh density, element type/shape function, and constitutive relation employed.

The Hertzian elastic contact model is the most widely used closed-form solution to calculate E of any material under generalized contact conditions. For small indentations ($h_{max} \ll R$), the paraboloidal indenter is well approximated as a sphere for which the Hertzian elastic solution exists. The relation between the depth of a spherical indenter and the corresponding applied load was formalized by Sneddon [20] based on the Hertzian formulation:

$$P_{sphere} = \frac{4}{3} \frac{E}{(1-v^2)} \sqrt{Rh^3} \qquad (1)$$

where v is the Poisson's ratio of the sample (equal to 0.5 for ideally incompressible materials, and assumed to be 0.49 for mathematical tractability in the simulations herein). Thus E can be calculated directly from the output $P–h$ response and chosen simulated R for a given material constitutive relation via Eq.

(1), although it is important to note that Eq. (1) tacitly assumes linear elastic behavior of a semi-infinite, indented material. The representative strain level ε applied to the material has been approximated in several forms, including: h/t, h/R and, most accurately, as

$$\varepsilon = 0.2a/R \qquad (2)$$

where a is the radius of contact at the material surface [21]. The fraction of indentation depth h to film thickness t sampled is not an actual strain and is termed hereafter as f, where the diameter of the elastically deformed contact zone and thus the propensity for artifactual stiffening in the $P–h$ response due to the underlying substrate increases with increasing f.

The polymeric films considered herein are modeled as both linear elastic and, separately, hyperelastic materials. For the linear elastic case, three values of E were considered: $E_1=100$, $E_2=10$, $E_3=0.5$ MPa. These values are based on the experimental results from Thompson et al., obtained via SPM-enabled nanoindentation (Si_3N_4 cantilever of $R=25$ nm) for thin film polyelectrolyte multilayers adhered to rigid (glass or polystyrene) substrates [4]. For the hyperelastic case, the strain energy
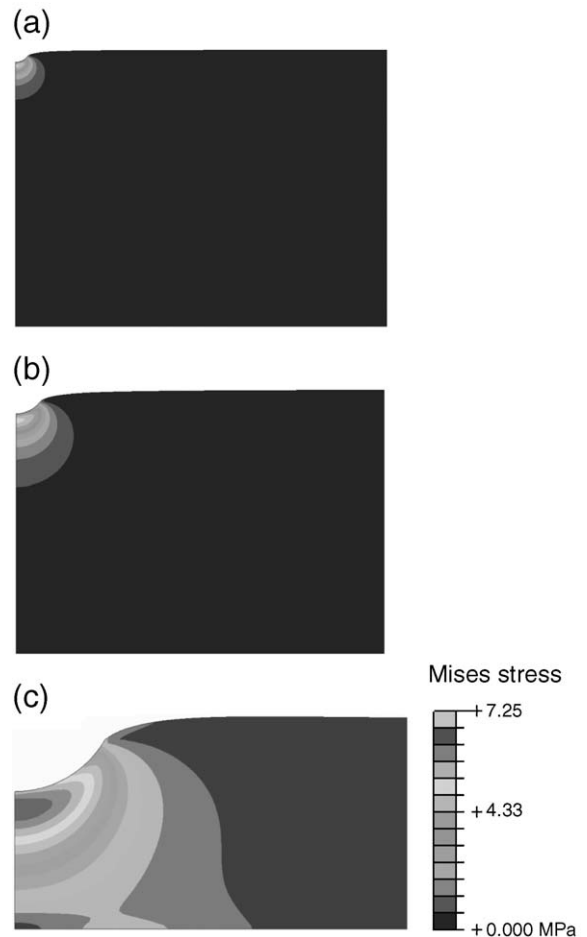
(a)

(b)

(c)

Fig. 3. Von Mises stress distributions for films of varying thickness t and $E=10$ MPa: (a) $t=1000$ nm, $h=20$ nm; (b) $t=600$ nm, $h=20$ nm; (c) $t=50$ nm, $h=17.5$ nm.

function W for incompressible materials was postulated by Mooney [22] and is given by

$$W = C_1(I_1-3) + C_2(I_2-3) \tag{3}$$

where C_1 and C_2 are the elastic constants and I_1 and I_2 are the first and second invariants of the Cauchy–Green deformation tensor [23].

Based on the above formulation, for an incompressible material with infinitesimal indentation depth h the Young's elastic modulus E can be expressed as

$$E = 6(C_1 + C_2). \tag{4}$$

Previous studies have shown that the widely applied infinitesimal strain models for nanoindentation yielded substantial errors in the estimated properties such as E for non-linear elastic materials [24]. The values for the elastic constants used in this hyperelastic analysis are $C_1 = 0.0235$ and $C_2 = 0.060$ MPa. These material constants are not chosen to represent a particular polymer, but rather to assess how the film thickness t and E independently affect the SPM-enabled nanoindentation response for a constitutive model that is more representative of polymeric materials than linear elastic models. The resulting value from Eq. (4) is $E = 0.50$ MPa, which is consistent with one of the three linear elastic cases considered, despite the clear difference in the constitutive relations.

For a given film thickness t, there exists a critical depth of indentation h_{cr} that depends on the mechanical properties of both the film and substrate, beyond which the force P required to attain a depth h increases due to the proximity of the film/substrate interface. This violates the semi-infinite film thickness ($t \gg h_{max}, R$) assumed by the Hertzian model, but h_{cr} is not easily identified a priori [3,25]. A semi-analytical correction for this artifactual increase in stiffness due to finite film thickness proposed by Dimitriadis et al. [5] as:

$$P = \frac{16}{9}E\sqrt{R\delta^3}[1 + 1.133\chi + 1.283\chi^2 + 0.769\chi^3 \\ + 0.0975\chi^4] \tag{5}$$

where

$$\chi = \sqrt{\frac{R\delta}{h}} \tag{6}$$

is the correction factor due to finite thickness. The maximum film thickness for which this correction is applicable is stated by Dimitriadis et al. as $h < 12.8R$ [5]. This restriction is based upon the assumption that the material behaves in a linear elastic manner for maximum strains less than or equal to 10%, which may or may not be true for a given material. According to this arbitrary limit, however, the thickness correction would apply for film thickness $t < 320$ nm in the current study. Eq. (5) can then be used to calculate E for films of ostensibly identical or systematically varied mechanical properties, of varying thickness. Mahaffy et al. [16] have shown that the value of the Poisson's ratio also affects the calculation of E when indenting samples of finite thickness. Experimental results [16] have
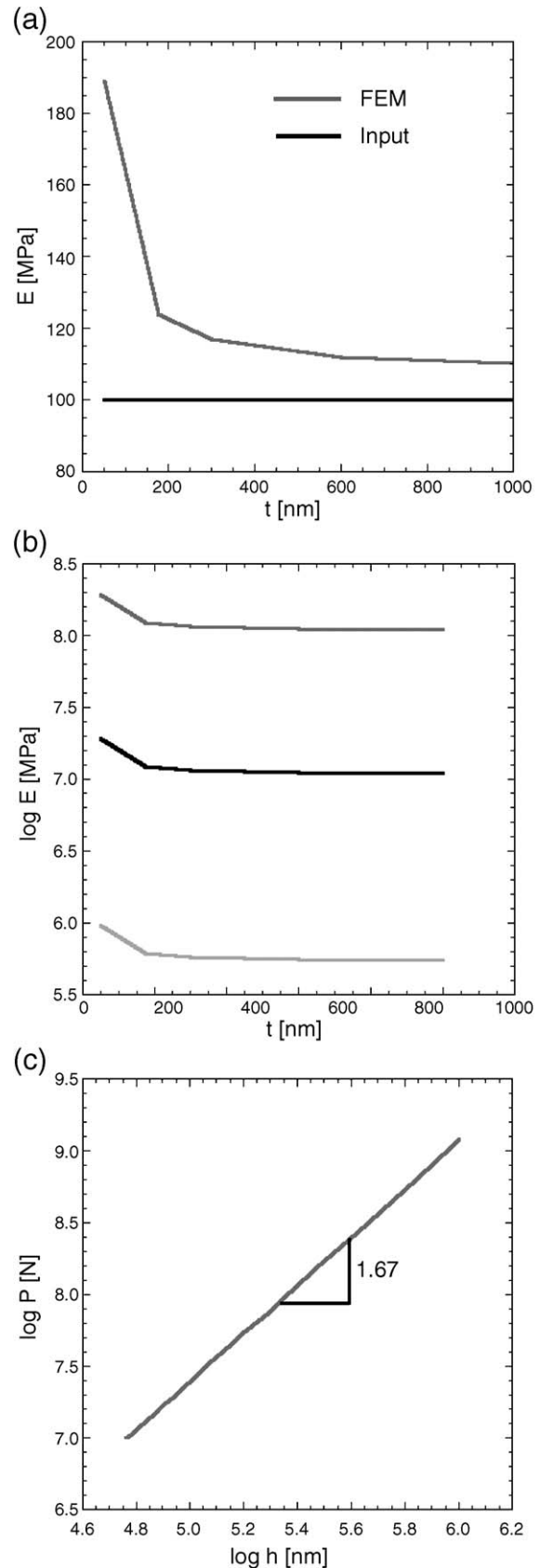
Fig. 4. Comparison of experimental and calculated E for linear elastic films as a function of film thickness t and constant indentation depth $h = 20$ nm: (a) $E = 100$ MPa; (b) $E = 100$, 10, and 0.5 MPa; (c) Deviation from Hertzian prediction of $3/2$ power law in Eq. (1) for $t = 50$ nm and $E = 100$ MPa.
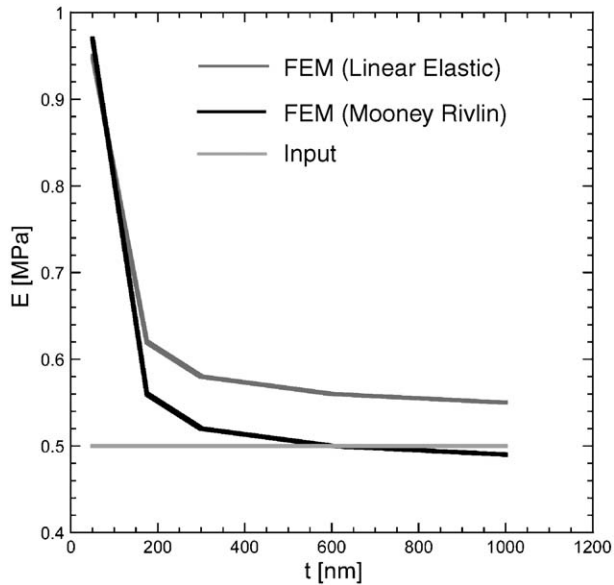
Fig. 5. Comparison of E calculated via Eq. (1), assuming either a linear elastic or a hyperelastic constitutive model (Mooney Rivlin, Eq. (4)) for $E = 0.5$ MPa.

shown that as the Poisson's ratio increases from 0.3 to 0.5, the depth h_{cr} at which the underlying stiff substrate artifactually stiffens the measured response actually decreases. This means that due to the high Poisson's ratio of polymers, even in micrometer-scale thick areas of experimental samples such as living cells, the Hertz model can fail to predict the elastic properties accurately.

3. Results

3.1. Effects of film thickness

Fig. 2a shows the variation of load P and depth h on a $\log_{10}$ scale for a simulated film of $t = 1000$ nm and $E = 0.5$ MPa. The calculated slope of $x = 3/2$ is consistent with the power law representation of Hertzian elastic contact (see Eq. (1)), and the value of E calculated via Eq. (1) is within 10% of the input value of E. This demonstrates the well-known result that for the case of linear elastic model of given E and sufficient film thickness t, the film-indenter contact can be well approximated by the Hertzian model. Note that the average or von Mises stress contours are confined well within the film as shown in Fig. 2b. Fig. 3a–c shows the von Mises stress distributions for the linear elastic case ($E = 10$ MPa) and a range of film thickness $t = 50$, 600, and 1000 nm. These simulations demonstrate the transfer of stresses through the thin films; for this value of E, the stresses are confined to ~10% of t for sufficiently large t ($t \sim 300$ nm, corresponding to a maximum nominal strain of 0.40). That is for a given critical thickness, E can be predicted to within 15% of the actual value via application of Eq. (1) and assumption of a linear elastic constitutive relation. When the thickness is below this critical value, the underlying rigid substrate induces overprediction of E, as shown in Fig. 4 a.

Fig. 4a shows the (linear elastic) E calculated from the P–h response via Eq. (1), as a function of t. This trend de-

monstrates the overestimation of E when the Hertzian model is assumed for finite film thickness and that, as t decreases with respect to h_{max}, there results a significant increase in calculated E with respect to the elastic modulus dictated by the simulated constitutive relation (i.e., the input or actual E of the indented material). As expected for a linear elastic analysis, this trend is similar for all values of E considered (Fig. 4b). This corroborates the fact that the value of E increases as the thickness is reduced for any value of E chosen. Fig. 4c indicates the corresponding deviation from the Hertzian contact power law value of $x = 3/2$. For the simulated film of $E = 100$ MPa, $x = 3/2$ for $t = 1000$ nm, but increases to $x = 5/3$ when the thickness is reduced to 50 nm. This deviation from the theoretical value underscores the lack of applicability of a model originally intended for macro-scale contact mechanics for linear elastic, semi-infinite material dimensions.
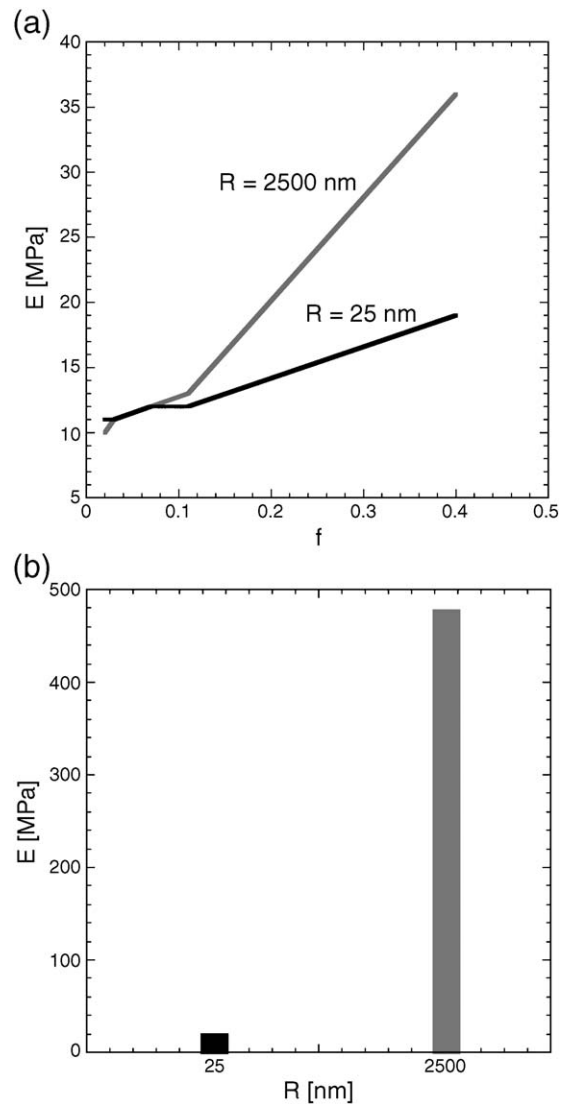

Fig. 6. Effect of indenter radius R on calculated E for an input modulus of 10 MPa: (a) as a function of the fraction of film thickness sampled $f = h/t$; (b) for a linear elastic film of $t = 50$ nm indented to a depth $h = 12.5$ nm with indenters of nanoscale and microscale radii. Note that the indenter of microscale radius significantly overestimates E due to substrate proximity effects.

3.2. Effects of elastic nonlinearity

In actuality, many polymeric materials exhibit highly nonlinear deformation even within the elastic regime [27]. This necessitates the need for understanding the nanoindentation P–h response through modeling of nonlinear constitutive relations. Here, the Mooney–Rivlin model has been applied to consider any differences in the stress transfer to the film/substrate interface and therefore in the associated P–h response as a function of elastic nonlinearities. Clearly, the overestimation of E due to finite t is very similar to that observed for the linear elastic case. These data demonstrate that elastic contact analysis with constitutive relations more representative of polymers predict the same effect of finite film thickness. Fig. 5 shows that the calculated E is close to the bulk or input value for $t > t_{cr} = 200$ nm and maximum indentation depth $h_{max} = 20$ nm ($\varepsilon_{max} = 0.40$). In addition, although the overprediction of E is observed for both linear elastic and hyperelastic models, Fig. 5 shows that the critical film thickness t_{cr} at which this overprediction occurs actually increases with respect to the linear elastic case for a given E and ε. In other words, nonlinear elastic deformation relaxes the film thickness constraint.

3.3. Effects of indenter radius

Fig. 6a shows the variation of E with respect to the dimensionless parameter $f = h / t$. While indenting samples that are of nanoscale thickness (~ 50 nm) or while indenting samples to $h > 0.1\,t$, the calculated E increases by more than a factor of two for $R = 2500$ nm when compared to $R = 25$ nm, for the same value of f. Even though the strains induced by the indenter with larger radius are much lower when compared to the strains induced due to smaller indenter [5], hence inducing lower stresses on the films, the calculated E are very high for larger radii. Fig. 6b shows the difference in modulus when a 50 nm thick sample is indented to a depth of 12.5 nm using indenters of radii $R = 25$ and $R = 2500$ nm. Fig. 7a shows the difference in calculated E when compared to an input or actual value of $E = 10$ MPa. Fig. 7b shows the P–h response for the bulk and $t = 50$ nm samples when indented to $h = 12.5$ nm. The stresses induced by the substrate proximity are mainly responsible for overprediction of E, as shown by Fig. 7b–d. This is clearly evident from the Mises stress profile in Fig. 7c and d, which show the von Mises stress profile where spheres of $R = 25$ and $R = 2500$ nm are used to indent a sample of $t = 50$ nm to an indentation depth of 12.5 nm. When indenting a sample to same indentation depth, the stresses induced by larger R (2500 nm) are lower compared to the smaller R (25 nm). However, the transfer of these stresses to the underlying substrate from larger indenter radii is increased significantly because the contact zone of elastic deformation is correspondingly larger. This very important fact brings out a unique correlation between the indenter geometry and shape of the stress contours for a given film thickness. As the indenter
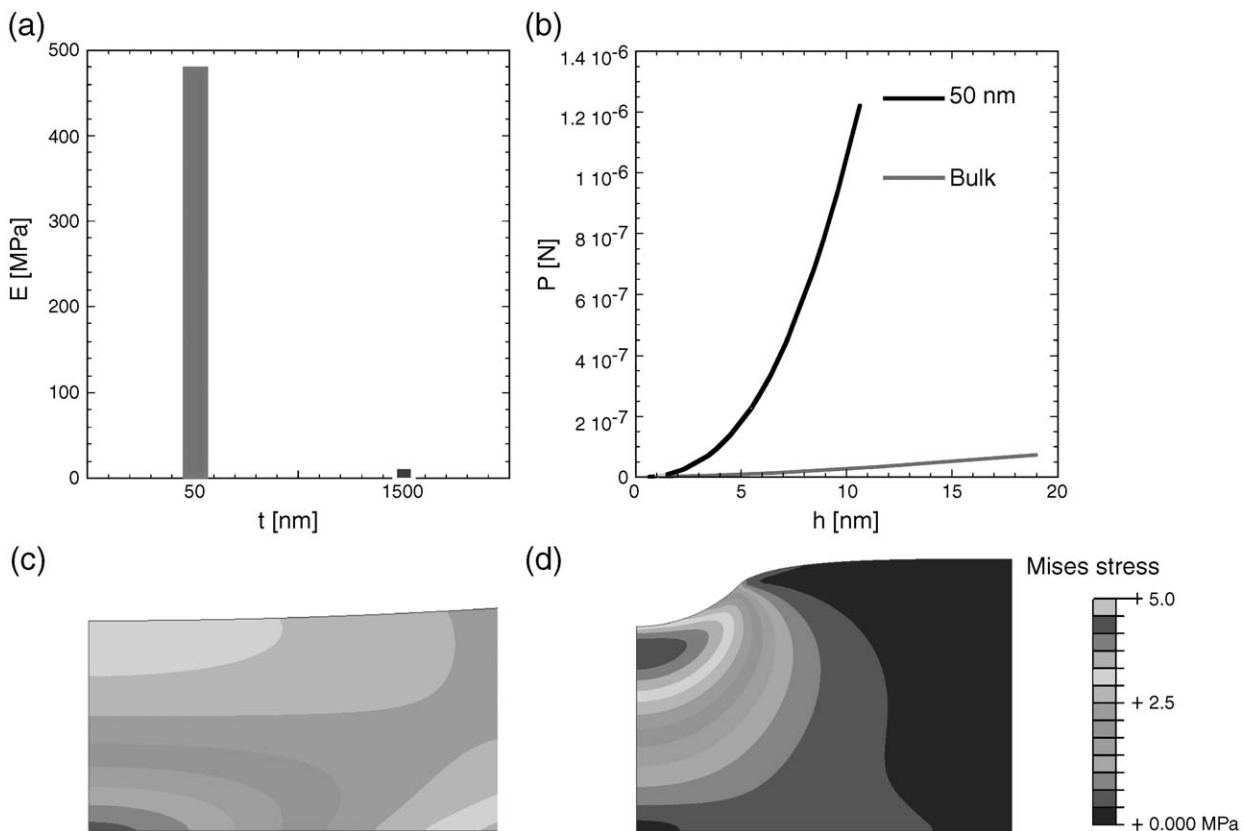

Fig. 7. Demonstration of substrate proximity effects on overestimation of thin film E, accentuated by the use of large indenter radii: (a) Calculated E for an input modulus of 10 MPa and indentation depth of 12.5 nm; (b) Corresponding load–depth (P–h) response compared to that of a bulk sample of same input modulus; Von Mises stress distribution for film thickness $t = 50$ nm and $h = 12.5$ nm for (c) $R = 2500$ nm; and (d) $R = 25$ nm.

geometry increases for a given indentation depth and film thickness, the stress distribution becomes flatter and asymmetrically distributed along the lateral direction with respect to the loading axis (see Fig. 7d). As films of nanoscale thickness that are strongly adhered to the substrate therefore resist lateral deformations during the indentation process, indentations of larger R induce comparably larger stress distributions within the film that approach and are distorted by the film/substrate interface. Thus, the P–h response from which E is calculated is affected at smaller h.

3.4. Applicability of Hertzian modifications

Certain semi-analytical models such as that of Dimitriadis et al. [5] directly consider the effects of finite thickness on mechanical properties estimated from the P–h response. Fig. 8 shows the comparison of the classical Hertzian model (Eq. (1)) with the Dimitriadis et al. model for a linear elastic material, indicating that calculated E increases with respect to "known" or independently assessed measures of E as t decreases. When compared to the Hertzian model, the Dimitriadis et al. model is superior in calculating film E. However, below a certain film thickness, the Dimitriadis et al. model also overestimates E. This comparison is important for two reasons. First, this shows that a model originally developed for macroscopic contact mechanics can be extended to linear elastic samples of finite thickness when a correction factor (of which the Dimitriadis et al. [5] and Mahaffy et al. [16] are two models) is used. Second, Fig. 7 shows that, even for linear elastic simplifications of polymer mechanical response, thickness-corrected Hertzian models also overestimate film E as t is reduced to the nanoscale.

Table 1 shows the effect of f on the amount of error in calculated E due to either large indentation depth or reduced film thickness. The results are tabulated for two indenter radii. Both the strain ε as well as simulated E increases as f increases. The error

Table 1
Effect of increase in f on contact strain ε and predicted E expressed as a function of indenter radius R

t [nm]	f	R [nm]	ε	E_{input} [MPa]	Overestimation of E [%]
18,000	0.03	2500	11.69	10	6
9000	0.07	2500	13.49	10	16
5250	0.11	2500	13.98	10	32
1500	0.40	2500	38.86	10	255
1000	0.02	25	28	10	10
600	0.03	25	28.29	10	12
300	0.07	25	28.26	10	16
175	0.11	25	30.25	10	24
50	0.35	25	43	10	89

becomes significantly high for $f > 0.1$, with percent error in E equal to 255% for $f = 0.4$ when $R = 2500$ nm and 89% for $f = 0.35$ when $R = 25$ nm. The significant increase in both ε as well as E for $R = 2500$ nm are due to the manner in which the plastic zone redistributes around the indentation zone, as shown in Fig. 7c.

Finally, it should be noted that these results include several simplifying assumptions, including axisymmetric (rather than fully three dimensional) deformation and neglect of linear/nonlinear viscoelastic effects.

4. Discussion

Recent engineering advances in materials processing have enabled fabrication of films with thickness that are on the order of 100 nm and less. These films have a wide range of applications including biological engineering substrata for fundamental studies of mechanically influenced cell function or for microelectronic insulators [7]. These examples are a small subset of emerging applications that require accurate mechanical characterization of the mechanical properties of polymeric thin films. The critical issue addressed in this study is the validity of the Hertzian model in estimation of E for polymeric thin films.

Fig. 3a–c shows clearly that the Hertzian model is valid below a critical film thickness t_{cr} for a given depth of indentation h_{max} and strain ε, provided that the film is a linear elastic solid. This immediately implies that application of the Hertzian model towards analysis of nanoindentation P–h responses can accurately estimate E for a given film thickness t that is deformed less than a critical depth of indentation h_{cr}. For the range of E considered, the critical thickness is approximately 20 nm, beyond which measured values of E can be within 15% of the input or actual bulk value. Outside of these conditions, there are several reasons for overprediction of E in application of the Hertzian model. These parameters are discussed below in the context of the simulated results.

While considering films which are of 1–100 nm in thickness, it is difficult both experimentally and theoretically to obtain precise calculated values of E with an indentation depth that is 10% of the film thickness (0.1 nm $< h_{\text{max}} < 10$ nm). This is demonstrated by the consideration of films for $t = 50$ nm in the present simulations; the power-law slope x increases from the analytically predicted value of $3/2$ to 1.6 when t is decreased from 1000 to 50 nm (Fig. 4c), and thus calculated E exceeds the actual value. The reason for this deviation is clear from Fig. 3,
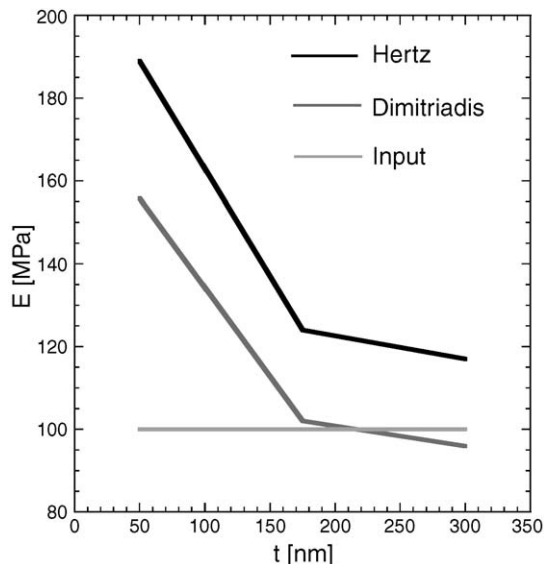

Fig. 8. Comparison of Hertzian and Dimitriadis models of elastic modulus calculation for input $E = 100$ MPa. Identical trends were observed for $E = 10$ and 0.5 MPa.

where it is seen that the stress field is not confined but rather includes the film/substrate interface. This shows that finite thickness can alter the stress and displacement field behavior, hence leading to overestimations of E. This becomes critical for application of nanoindentation experiments in applications of polymeric films as cell substrata, as it is known that substratum compliance contributes significantly to cell morphology and physiology [4,28]. The same trend that is observed for the linear elastic case is also seen for the hyperelastic case, where (material) elastic nonlinearity can be incorporated to simulate polymeric responses more accurately. Even for the case of the hyperelastic model chosen, the Hertzian prediction of E exceeds the actual value by a factor of two below a certain t_{cr}. The maximum strain in the loading direction for the case of $E = 0.5$ MPa is shown in Fig. 5 for both linear elastic and hyperelastic models: the t_{cr} for hyperelastic case is reduced to 200 nm compared to linear elastic model ($t_{cr} = 300$ nm). This means that if Hertzian elastic analysis is applied to analyze the mechanical properties of hyperelastic thin films, these films can be indented to a greater fraction of the film thickness f (and to a larger ε) without inducing overpredictions due to finite film thickness.

Fig. 7c–d demonstrates that even though indenters with larger radii R induce smaller indentation strains for a given indentation depth h, the transfer of these stresses to the substrates for large R is much more pronounced. Perhaps counterintuitively, this indicates that lower effective contact strains – even those within the elastic limit of the film material – do not necessarily imply more accurate measurements of E for polymeric thin films. In fact, the overestimation of E increases with increasing R for $h > t_{cr}$ as shown in Fig. 6a–b.

Despite this potential artifact of large indenter radii R, in order to apply strains within the linear range of material deformation during nanoindentation, it is often necessary to use probes with large radius, e.g., micrometer-scale spheres for nanoscale film thicknesses [5]. This is often not feasible with Si_3N_4 or Si cantilevers suitable for SPM imaging, as the cantilever tips of such probes exhibit R on the order of 25 nm and thus induce $\varepsilon > 10\%$ for indentation depths $h < 20$ nm. For such probe geometries, the Hertzian model would apply for $t > 300$ nm, below which E values are overestimated by a factor equal to or greater than 20% as shown in Fig. 4a. This overestimation for decreasing t is due to the fact that the strains exceed the infinitesimal range and thus invalidates the small-strain approximations inherent in the Hertzian model, independent of finite film thickness effects. However, it is important to note that this overestimation as shown in Table 1 is not predicted to exceed 89% for nanoscale films, indicating that changes greater than this could be attributed either to real microstructural changes or to other experimental/material artifacts other than film thickness t.

5. Conclusions

Together, these systematic simulations of contact-enabled mechanical characterization for compliant thin films indicate three key features. First, in order for elastic modulus E to be accurately determined for any polymer film thickness t, strain magnitude ε, and fraction of film thickness sampled f, analytical models must include both finite film thickness and nonlinear elastic deformation. Second, even when ε and h/t exceed nominal levels required for small strain and semi-infinite thickness approximations to apply, linear elastic and hyperelastic descriptions of these polymer thin films indicate an artifactual increase on the order of a factor of two. Third, although the choice of large indenter radius R is suitable to minimize contact strain ε, large R also confers large strain volumes within the film that exacerbate finite film thickness effects and can thus be counterproductive in SPM-enabled estimates of mechanical compliance for nanoscale polymeric films.

References

[1] M.C. Berg, S.Y. Yang, P.T. Hammond, M.F. Rubner, Langmuir 20 (2004) 1362.
[2] J.D.Y. Mendelsohn, S.Y. Hiller, A.I. Hochbaum, M.F. Rubner, Biomacromolecules 4 (2003) 96.
[3] R. Saha, W.D. Nix, Acta Mater. 50 (2002) 23.
[4] M.T. Thompson, M.C. Berg, I.S. Tobias, M.F. Rubner, K.J. Van Vliet, Biomaterials 26 (2005) 6836.
[5] E.K. Dimitriadis, F. Horkay, J. Maresca, B. Kachar, R.S. Chadwick, Biophys. J. 82 (2002) 2798.
[6] J. Domke, M. Radmacher, Langmuir 14 (1998) 3320.
[7] A.J. Engler, L. Richert, J.Y. Wong, C. Picart, D.E. Discher, Surf. Sci. 570 (2004) 142.
[8] H. Hertz, J. Reine Angew Math. 92 (1882) 156.
[9] J.B. Pethica, R. Hutchings, W.C. Oliver, Philos. Mag., A 48 (1983) 593.
[10] M.F. Doerner, W.D. Nix, J. Mater. Res. 1 (1986) 601.
[11] J.A. Tayler, J. Vac. Sci. Technol., A 9 (1991) 2464.
[12] M.T. Kim, Thin Solid Films 283 (1996) 12.
[13] W.C. Oliver, G.M. Pharr, J. Mater. Res. 7 (1992) 1564.
[14] W.T. Chen, Int. J. Eng. Sci. 9 (1971) 775.
[15] W.T. Chen, P.A. Engel, Int. J. Solids Struct. 8 (1972) 1257.
[16] R.E. Mahaffy, S. Park, E. Gerde, J. Kas, C.K. Shih, Biophys. J. 86 (2004) 1777.
[17] R. Ludovic, A.J. Engler, D.E. Discher, C. Picart, Biomacromolecules 5 (2004) 1908.
[18] T.Y. Tsui, J. Vlassak, W.D. Nix, J. Mater. Res. 14 (1999) 2196.
[19] ABAQUS/Standard, v6.4-1, ABAQUS Inc., 2005.
[20] I.N. Sneddon, Int. J. Eng. Sci. 3 (1965) 47.
[21] D. Tabor, The Hardness of Metals, Clarendon Press, Oxford, 1951.
[22] M. Mooney, J. Appl. Phys. 11 (1940) 582.
[23] A.E. Green, W. Zerna, Theoretical Elasticity, Clarendon Press, Oxford, 1968.
[24] K.D. Costa, F.C.P. Yin, J. Biomech. Eng. 121 (1999) 462.
[25] K.J. Van Vliet, Ph.D. Thesis, Massachusetts Institute of Technology, Cambridge, 2002.
[26] Y.O. Tu, D.C. Gazis, J. Appl. Mech. 31 (1964) 659.
[27] Y.C. Fung, Biomechanics: Mechanical Properties of Living Tissues, Springer-Velag, New York, 1981.
[28] P.J. Pelham, Y.L. Wang, Proc. Natl. Acad. Sci. 94 (1997) 13661.